J. Bangladesh Acad. Sci. 49(1); 35-44: June 2025 DOI:https://doi.org/10.3329/jbas.v49i1.76026

Journal of Bangladesh Academy of Sciences

Journal homepage: http://www.bas.org.bd/publications/jbas.html

Research Article

Studies on the vorticity of superconducting 3D Nano-sized pyramidal samples as a function of coherence length

Sharmin Aktar and Abul Hasnat*

Department of Physics, Jagannath University, Dhaka, Bangladesh

ARTICLE INFO

Article History

Received: 20 August 2024
Revised: 13 January 2025
Accepted: 15 January 2025

Keywords: Mesoscopic, Superconductor, Pyramidal, GL formalism, Vortex.

ABSTRACT

This study examines the vorticity of a nano-sized superconducting pyramidal sample using the 3D Ginzburg-Landau (GL) formalism, a crucial tool for analyzing the nonuniform geometrical sample. We consider a field applied perpendicularly to the pyramid's base and characterize the sample's static properties as a function of its coherence lengths. The study focuses on the vortex nucleation point (vortex penetration field) and the vortex configuration within the sample. The sample's free energy, magnetization, and other steady properties are measured on the plane orthogonal to the field with the applied magnetic field increases. We examine two samples with different dimensions, one equal to 12ξ and the other 6ξ. The study investigates the variation of the Meissner state's stability range and the critical field of the pyramidal sample as a function of the sample size.

Introduction

A field within condensed matter physics, known as mesoscopic physics, focuses on studying materials of intermediate sizes (Alegria et al., 2021). These materials can range in size from the nanoscale, which is just a few atoms (e.g., a molecule), to micrometers. The size of mesoscopic samples is typically similar to the coherence length (ξ) and/or magnetic field penetration depth (λ) (Ge et al., 2023). This sample size significantly affects the sample characteristics under an external magnetic field (H) (Taupin et al., 2016), and the presence of this factor can create several superconducting states, along with phase transitions. Variations in the temperature (T) or the applied magnetic field to the mesoscopic sample can cause magnetization jumps (Geim et al., 1997).

Research has been previously conducted on mesoscopic superconductor's magnetic response with different geometries: (i) disk-shaped samples (Deo et al., 1997; Zharkov et al., 2000), (ii) indefinitely long cylinders (Zharkov et al., 2000), (iii) ring-like structures (Baelus et al., 2001), and more complex geometries (Fomin et al., 1998). The Ginzburg-Landau (GL) theory forms the basis for the theoretical study of mesoscopic superconductors, providing a satisfactory explanation for mesoscopic samples across a wide range of magnetic fields and temperatures (De Gennes, 2018). Typically, disks or cylindrical geometries of mesoscopic superconducting samples enclosed by an insulator or vacuum exhibit two types of superconducting states. A circularly symmetric state with a fixed angular momentum value is one form among them, known as a "giant vortex." Important issues regarding magnetic properties and phase transitions in certain geometrical systems should be addressed, including basic and technological aspects.

*Corresponding author:<abul.hasnat@phy.jnu.ac.bd>

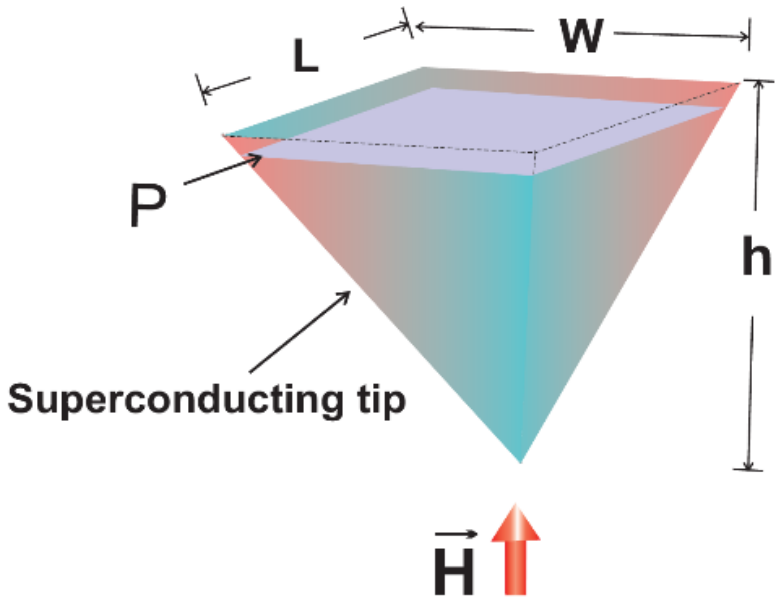

Fig. 1. Superconducting pyramidal sample in the presence of an applied magnetic field where the field is perpendicular to the base plane of the sample. Here, L, W, and h represent the tip's length, width, and height, and in this case, L=W=h. We are considering two samples, one with all dimensions (L, W, h) equal to 6ξ and another with all dimensions equal to 12ξ.

Understanding the process of magnetization in type-II superconductors depends largely on the dynamics of magnetic vortices. The relationship between the vortices and sample surfaces and the sample shape decreases with sample size. Various research studies have focused on magnetizing a mesoscopic superconductor without pinning centers (Baelus et al., 2004). Calculations indicate transitions between various large vortex states in mesoscopic type-I superconducting thin films, with multi-vortex states being mostly metastable, although occasionally thermodynamically stable states are also observed. Mesoscopic triangular cylinders of type-I samples reveal a vortex-antivortex molecule (Misko et al., 2003).

The effect of surface defects and sample geometry on vortex dynamics was examined using a finite element method to solve the TDGL equations (Kim et al., 2007). The mixed state in the mesoscopic cylindrical sample made of type-II superconducting materials shows that as the system searches for the configuration with the lowest Gibbs free energy, it passes through nearly stable intermediate states. The sample's square symmetry aligns with the steady-state arrangement. Several bulk superconductor experiments (De Gennes 1965; Fink and Presson, 1969) investigated the influence of sample surfaces on the first vortex entry.

According to Deo et al. and Schweigert et al., Phase transitions of the first order take place between large vortices with different angular momentum, causing the observed magnetization jumps (Deo et al., 1997). Second, in samples with sufficiently large radii, multivortex structures (Schweigert et al., 1998) can form, which are comparable to the bulk superconducting material's Abrikosov flux line lattice. These states are a mixture of different angular momentum vortex states. An effective total angular momentum or vorticity can also be introduced for multi-vortex states. Phase transition of the second order occurs with changing the magnetic field, bringing about a switch between the multi-vortex states (MVSs) and giant vortex states GVSs) (Baelus and Peeters, 2002; Wang and Wang, 2019).

The boundary effect significantly impacts the charge distribution in such mesoscopic samples. Furthermore, the sample's screening currents cause charge redistribution, resulting in a nonuniform distribution even in the Meissner state. This scenario is similar to an inverted vortex, with its core extending to infinity. When vortices exist, the Meissner charge interacts with the previously investigated vortex charge (Meissner and Ochsenfeld, 1933; Maxwell 1950; Bardeen et al., 1957), which is specific to mesoscopic samples. We conducted a theoretical investigation into electrical charge redistribution that occurs in various geometries of mesoscopic superconducting samples, such as disks and cylinders. Recent improvements in microfabrication and experimental techniques have focused emphasis on mesoscopic superconductors. Important basic and technological problems about magnetic characteristics and phase transitions in such small, constrained systems must be addressed.

In samples of comparable size to the coherence length, the layout of the vortices is determined by the confinement of the superconducting condensate. In previous studies, researchers have explored the shapes of disks within the framework of the Linearized GL equation. They assumed a uniform magnetic field within the disks. P. Singha Deo, V. A. Schweigert, F. M. Peeters and A.K. Geim (Deo et al., 1997) examined the magnetization curve of mesoscopic disks with finite thickness changes with the external magnetic field. Several experimental techniques have been devised to observe these unique states, but none of them have been able to distinguish between MVSs and GVSs.

Mel'nikov et al. developed a comprehensive numerical model to describe the vortex state of FFS using the time-dependent Ginzburg-Landau (TDGL) theory (Mel'nikov et al., 2002). They also introduced a symmetry-based approach to analyze vortex molecules and complexes through analytical studies. Their simulations allowed for a thorough analysis of the nonlinear region at low fields.

Because the shape of a mesoscopic sample differs from the Abrikosov lattice triangle, the vortex patterns prominently display aspects of the sample's shape instead of the triangular lattice, leading to powerful finite-size effects and significant shape effects determining vortex configurations. For example, as proven theoretically (Baelus et al., 2001; Baelus et al., 2004) and experimentally (Grigorieva et al., 2006), vortices in mesoscopic disks create circular symmetric shells that are size-dependent (Misko et al., 2007). When confined, small disks can cause vortices to transform into large vortexes (GV) due to strong confinement effects. Among mesoscopic superconductors of different shapes, triangles are noteworthy. The symmetry of quilateral triangles and the Abrikosov vortex lattice is the same. This implies that a triangle can accommodate part of the vortex lattice without distortion for a given number of vortices. Therefore, vortex patterns in the shape of triangles are much more stable because the interaction between vortices and boundary effects enhances their stability (Zhao et al., 2008).

A magnetic field's existence influences superconductivity behavior in small equilateral triangles, squares, and other configurations while maintaining the symmetry (C3, C4) of the boundary conditions (Chibotaru et al., 2001). This can result in a new vortex configuration surrounding a single antivortex. Researchers have studied the behavior of type II mesoscopic superconducting spheres with an externally applied magnetic field (Baelus et al., 2007). They studied the stable vortex states in these spheres at different radii. A study by A. Hasnat explored how the pyramidal topology of a superconductor affects vortex formation and stability (Hasnat, 2020).

One of the popular theories used to describe the magnetic behavior of superconductors is the Ginzburg-Landau (GL) theory, the time-dependent version of it is generally called the time-dependent Ginzburg-Landau theory (TDGL). Computational analysis involves using finite-element discretization of the TDGL equations (Tinkham, 2004). These methods are recognized as powerful computational

tools for approximating solutions to partial differential equations, especially for samples with complex shapes.

In Fig. 1, the superconducting pyramidal sample is displayed with the observation plane (P) indicated when a magnetic field is applied. The superconducting properties of a 3D inhomogeneous sample can be observed more easily using the GL formalism than with the other tools. The pyramidal shape of the superconducting sample is unique in terms of its applicability. Pyramidal samples have a higher critical field value than their bulk materials. STM's scanning tip could have a pyramidal form. The major goal of this research is to investigate the magnetic, thermodynamic, and critical phenomena of superconducting pyramidal samples using the 3D GL formalism. Free energy, Cooper pairs density, magnetism, and screening current density will all be examined in terms of coherence length. The variance in coherence length determines the quality of the various sample materials. We want to connect the coherence duration with the sample's Meissner state. We want to determine under what conditions the Meissner state and critical current will be enhanced.

Theoretical formalism

A nano-sized superconducting sample is placed within an insulator media under a homogeneous, perpendicular applied magnetic field $\vec{H}$. By applying the dimensionless variables, we obtain the following form of 3D GL equations:

$$(-i\vec{\nabla}_{3D}-\vec{A})^2\psi = \psi(1- |\psi|^2),$$

$$-k^2\Delta\vec{A} = J_{3D} = \frac{1}{2i}\left(\psi^*\vec{\nabla}_{3D}\psi - \psi\vec{\nabla}_{3D}\psi^*\right) - |\psi|^2\vec{A},$$

$$\vec{n}.\left(-i\vec{\nabla}_{3D} - \vec{A}\right)\psi|_{boundary} = 0.$$

The superconducting electron is represented by $\psi(\vec{r}) = |\psi|\exp(i\phi)$, where ψ denotes the superconducting complex order parameter with the magnitude value of $|\psi|$ and with its phase ϕ. The value of $|\psi^*\psi|$ is nearly equivalent to the superconducting electrons' number, N_s, at a position $\vec{r}$. The supercurrent that runs through the material below Tc is represented by the phase ϕ ($\vec{r}$). The coherence length (ξ) determines the distance, and the order

$$[(-i\vec{\nabla}_{3D} - \vec{A})^2\psi_0 - \overline{\psi_0} + |\psi_0|^2\psi_0] = \eta(\psi - \psi_0)$$

The boundary conditions at the sample boundaries cause the normal component of the superconducting current to become zero. To solve the GL equations, we use a uniform grid space (in Cartesian x, y, z coordinates) with 5 grid points at every unit of ξ distance and a superconductor area of 63×63×63 grid points. Next, we use an iterative procedure based on the link variable approach and the Gauss-Seidel technique to determine the order parameter (ψ). The iterative process is directed in the following manner:

Here, η is the real coefficient ψ, and ψ_0 is the best approximation of the current and next iteration.

Using a link variable approach,

$$U_\mu^{\vec{r}_1,\ \vec{r}_2} \equiv \exp[-i\int_{\vec{r}_2}^{\vec{r}_1}\vec{A}_\mu(\vec{r}).d\vec{\mu}]$$

$$[-\psi_0 + |\psi_0|^2\psi_0 - \frac{1}{U_\mu}\frac{\partial^2}{\partial\mu^2}(U_\mu\psi_0)] = \eta(\psi - \psi_0)$$

with μ = x, y and z

The essential numerical technique is to find words that go along with the new answer for ψ and to evaluate based on ψ_0

$$[\eta - (1-T)\frac{4}{d^2} + 2|\psi_0|^2]\psi = \widetilde{U}\psi_0 + \eta\psi_0 + 2\psi_0|\psi_0|^2 - {\psi_0}^2\psi^*$$

and solution

Here, ξ, λ and H_{c2} indirectly depend on the temperature:

$$c\psi - a + e\psi^* = 0$$

$$\xi(T) = \frac{\xi(0)}{\sqrt{1 - T/T_{c0}}}$$

$$\lambda(T) = \frac{\lambda(0)}{\sqrt{1 - T/T_{c0}}}$$

$$H_{c2}(T) = H_{C2}(0)(1 - \frac{T}{T_{C0}})$$

In our work, we considered two samples in terms of the different coherence lengths, such as one sample with the materials of 12ξ and the other 6ξ. Here the working temperature is considered at $t=T/T_{c0}=0.9$. We characterize the sample's properties with varying fields. Our main focus is to observe the changes in free energy in those fields.

Results and Discussion

We would like to investigate the static properties of the pyramidal mesoscopic samples. Pyramidal geometry has some unique advantages, the critical field of the pyramidal sample is enhanced than the bulk sample materials. We would like to observe the basic superconducting features such as the Cooper pairs density, screening current density, critical parameters, etc. Our results obtained are represented as follows. The free energy of the sample conveys a lot of crucial information about it; we start with the free energy curve here. In Fig. 2, the 12ξ sample's free energy has been shown with respect to the applied field. We observe that the free energy changes are continuous with varying fields, which expresses that there is no penetrating flux as a form of vortex (zero vorticity, L=0) inside the sample. This definite sample size and coherence length do not permit the nucleation of the vortex up to the point of the transition field. We did not observe the vortex in the 3D iso-surface plot in the entire range of free energy. The combined effect of these sample sizes and coherence length provides an extremely large Meissner state of the sample, which has some practical applications, such as the STM tip being used in the dissipationless regime.

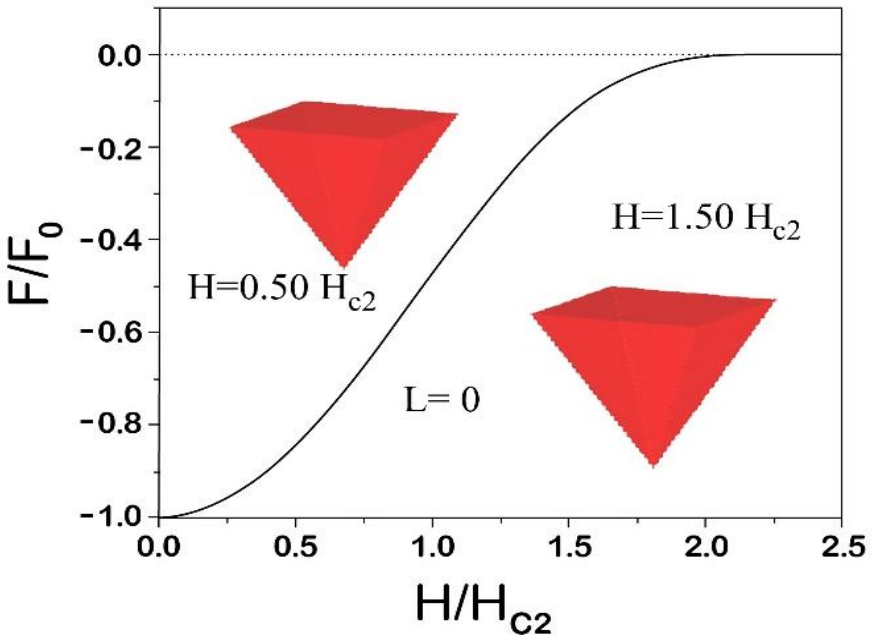

Fig. 2. Free energy changes with the applied field of the 12ξ sample. The inset shows the 3D iso-surface plot of the sample at the field $H/H_{c2}=0.50$ and $H/H_{c2}=1.50$. Here L denotes vorticity. The dotted line on the upper portion of the plot shows the superconducting state to the normal state transition point.

Magnetization vs. the applied field graph of 12ξ sample is shown in Fig. 3. The magnetization is increased up to the field $H \approx 1.00H_{c2}$. No jump (discontinuities) is observed in the curve, indicating that no vortex penetrated the sample in the entire range of the applied field. We didn't observe any paramagnetic effect as magnetization never takes the positive value.

Distribution of (a-b) the Cooper pairs density and (c-d) screening current density at the field of $H=0.50H_{c2}$ and $H=1.50H_{c2}$, respectively are shown in Fig 4. The Measurements are taken on the base plane of the pyramid since this plane is in orthogonal alignment with the applied field. (a) There is a uniform distribution

of the Cooper pairs density at field $H=0.50H_{c2}$, and (b) the Cooper pairs are less suppressed in the middle part than the edges part of the sample at field $H=1.50H_{c2}$. On the other hand, (c-d), the screening current density starts generating from the edges part of the sample, and the screening current gradually increases when the field increases. At the four corner edges of the sample, the screening current is considerably less than in other parts of the sample.

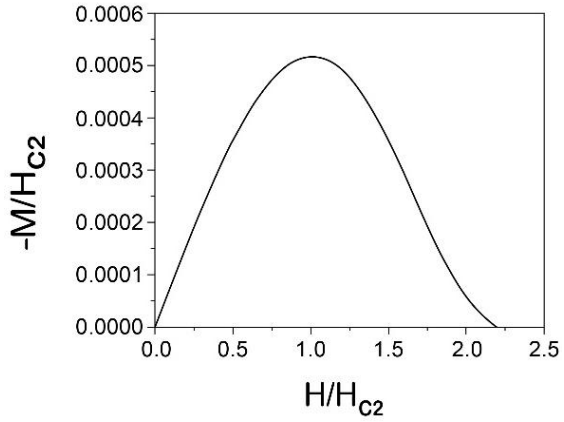

Fig. 3. 12ξ sample's magnetization changes with the applied field.

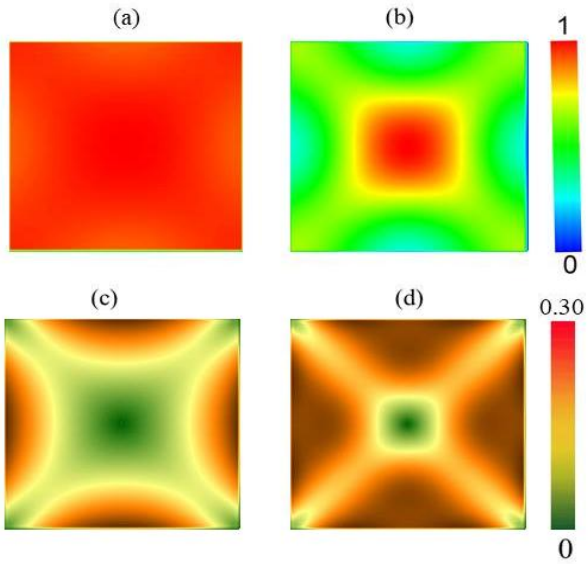

Fig. 4. (a-b) Cooper pairs density and (c-d) screening current density of 12ξ sample

6ξ sample's free energy vs. the applied field graph is shown in Fig. 5 (a). The dotted line specifies the transition point from the superconducting state to the normal state. Discontinuities are observed in the free energy graph, which indicates that the vortex appeared in this sample. The stability ranges of the distinguished vortex states are clearer in the magnetization curve (Please see in Fig. 6). 3D iso-surface plot of the sample at different vortex states such as L=1, 2, 3, and 4. 3D iso-surface plot of the sample at different vortex states such as L=1, 2, 3 and 4 are also shown in the right panel of the Fig. 5 (b-e). (b-e) vortex is visualized, and the separated vortex can be seen clearly in the 3D representation of the sample's iso-surface plot.

The Meissner state's stability range in the sample is observed at about $\Delta H \approx 0.55\ H_{c2}$, with the critical field at around 1.78 Hc2.

Magnetization of the 6ξ sample variation with the applied field is shown in Fig. 6. Discontinuities for the different vortex states in the magnetization are clearer than the free energy curve. The odd vortex states' stability range is shorter than the even number vortex states since the even number vortex states are energetically favorable for this pyramidal-shaped sample. The stability range of the L=4 state is greater than all states. Only paramagnetic effects are overserved. The magnetization of 6ξ is higher than the 12ξ sample.

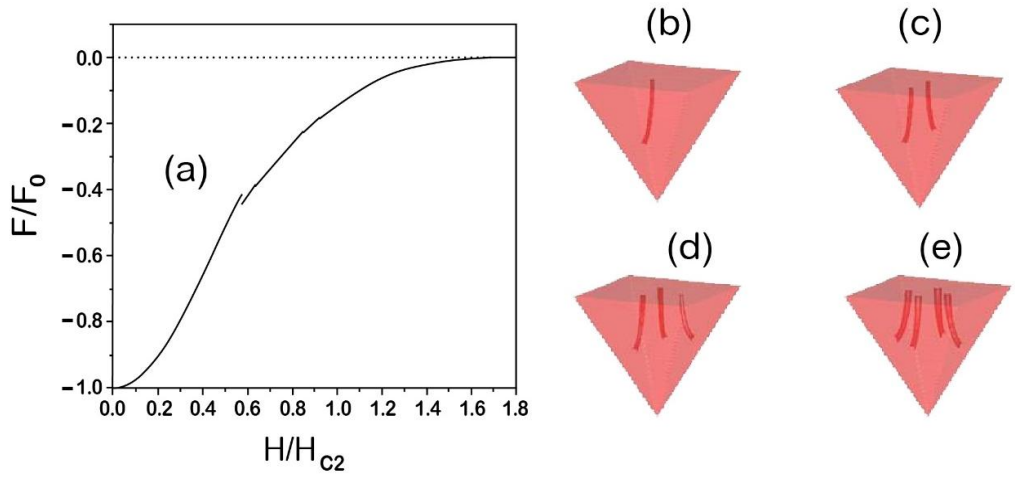

Fig. 5. (a) Free energy changes with the applied field of the 6ξ sample. (b-e) 3D iso-surface plot of the sample at distinguish vortex states such as L=1, 2, 3, and 4.

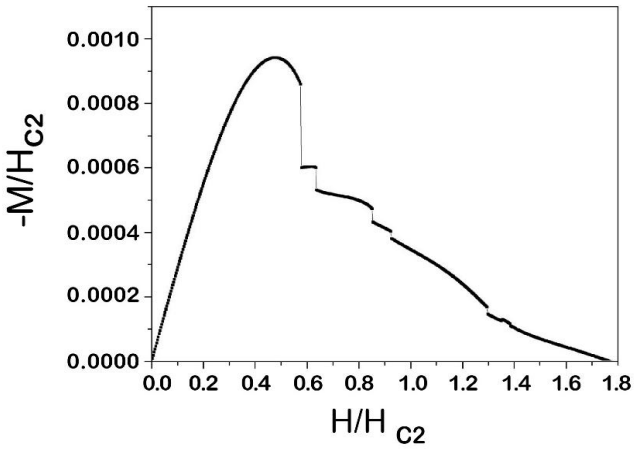

Fig. 6. Magnetization variation with the applied field of 6ξ sample. Discontinuities indicate the change of vortex states.

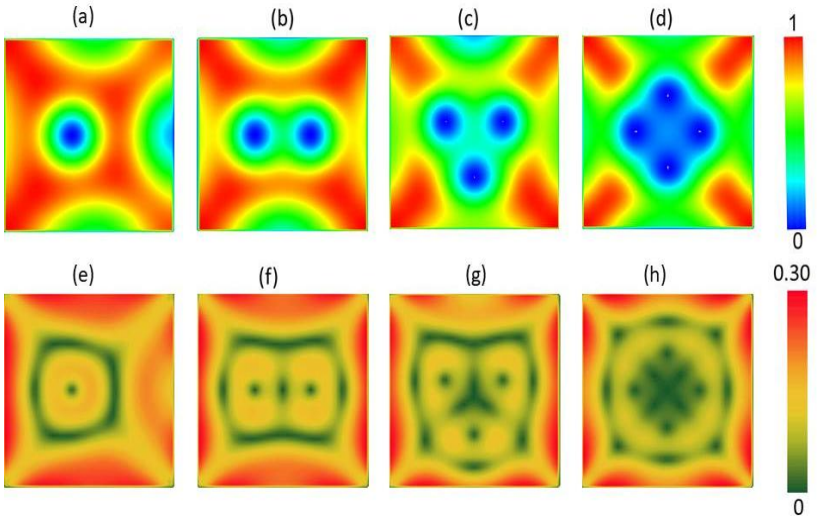

Fig. 7. Contour plots of (a-d) Cooper pairs density and (e-h) screening current density of 6ξ sample at L=1 to 4 vorticity, respectively.

Contour plots of Cooper pairs density and screening current density of 6ξ sample at different vortex states, L=1 to 4, are shown on the base plan of the pyramid in Fig. 7, respectively. The value of the color is given on the corresponding color bar. Multi-vortex states are clearly observed from the contour plots. The Cooper pairs are completely suppressed in the center of every vortex and the distribution of the Cooper pairs are higher where the screening current is lower and vice versa, these are the fundamental properties. In the four corner edges of the pyramid, the Cooper pairs are higher than those of the side region due to the strong superconducting region. In the L=2 state, the second vortex comes from the other side of the same axis of the sample, and the two vortexes take a straight position.

At the L=3 state, the third vortex enters from another axis and forms the triangular arrangement of the vortex. At the L=4 state, a square arrangement of the vortex is formed. At L=2, 4 states, there are symmetric arrangements of the vortex which gives the enhance stability range than the odd vortex states. In every vortex core, there is a whirl current in it. The screening current density on the edges of the sample is greater than the corners of the sample. This strong screening current presses the vortices to the center with increasing field.

Conclusions

The vorticity of a superconducting 3D nano-sized pyramidal sample is observed within the Ginzburg-Landau (GL) formalism. Stationary properties such as Cooper pairs density and screening current density of the sample are studied in detail. Free energy and magnetization are calculated based on the varied applied fields. The variation of the vorticity with the different coherence lengths (ξ) is investigated. No vortex is observed (L=0; here, L is vorticity) in the sample with 6ξ dimension, but in the sample with 12ξ, L_{max}= 7 is observed. Separated vortex (multi-vortex states) is clearly visible in the iso-surface plot obtained from the 3D data of $|\psi|^2$. Only a paramagnetic response is observed by analyzing the sample's magnetization.

Acknowledgement

Thanks to the Department of Physics, Jagannath University, for allowing us to conduct this research work.

Author's Contribution

Abul Hasnat Rubel: Planning the research work, writing – original draft, Corresponding author.

Sharmin Aktar: Running the code, data management, plotting graphs.

Declaration of conflicting interests

The authors have no conflicts to disclose.

References

Alegria LD, Bøttcher CG, Saydjari AK, Pierce AT, Lee SH, Harvey SP, Vool U and Yacoby A. High-energy quasiparticle injection into mesoscopic superconductors. *Nature Nanotechnology*. 2021; 16(4): 404-408.

Baelus BJ, Cabral LR and Peeters FM. Vortex shells in mesoscopic superconducting disks. *Phys. Rev. B.* 2004; 69(6): 064506.

Baelus BJ, Peeters FM and Schweigert VA. In superconducting disks and rings, there are Saddle-point states and energy barriers for vortex entrance and exit. *Phys. Rev. B.* 2001; 63(14): 144517.

Baelus BJ and Peeters FM. Dependence of the vortex configuration on the geometry of mesoscopic flat samples. *Phys. Rev. B.* 2002; 65(10): 104515.

Baelus BJ, Sun D and Peeters FM. Vortex structures in mesoscopic superconducting spheres. Condensed matter and materials physics. *Phys. Rev. B.* 2007; 75(17): 174523.

Bardeen J, Cooper LN and Schrieffer JR. Theory of superconductivity. *Phys. Rev.* 1957; 108(5): 1175.

Chibotaru LF, Ceulemans A, Bruyndoncx V and Moshchalkov VV. Vortex entry and nucleation of antivortices in a mesoscopic superconducting triangle. *Phys. Rev. Lett*. 2001; 86(7): 1323.

De Gennes PG. Superconductivity of metals and alloys. *CRC press*. 2018. p 292.

De Gennes PG. Vortex nucleation in type II superconductors. *Solid State Commun.* 1965; 3(6): 127-130.

Deo PS, Schweigert VA, Peeters FM and Geim AK. Magnetization of mesoscopic superconducting disks. *Phys. Rev. Lett.* 1997; 79(23): 4653.

Fink HJ and Presson AG. Stability limit of the superheated Meissner state due to three-dimensional fluctuations of the order parameter and vector potential. *Phys. Rev*. 1969; 182(2): 498.

Fomin VM, Misko VR, Devreese JT and Moshchalkov VV. Superconducting mesoscopic square loop. *Phys. Rev. B.* 1998; 58(17): 11703.

Ge JY, Gladilin VN, Van de Vondel J and Moshchalkov VV. Vortex matter and critical magnetic fields in mesoscopic superconducting strips. *Supercond. Sci. Technol*. 2023; 36(8): 085014.

Geim AK, Grigorieva IV, Dubonos SV, Lok JG, Maan JC, Filippov AE and Peeters FM. Phase transitions in individual sub-micrometre superconductors. *Nature.* 1997; 390(6657): 259-262.

Grigorieva IV, Escoffier W, Richardson J, Vinnikov LY, Dubonos S and Oboznov V. Direct observation of vortex shells and magic numbers in mesoscopic superconducting disks. *Phys. Rev. Lett.* 2006; 96(7): 077005.

Hasnat A. Vortex configurations of a nano-sized superconducting 3d pyramidal confinement. *J. Supercond. Nov. Magn*. 2020; 33(3): 575-582.

Kim S, Burkardt J, Gunzburger M, Peterson J and Hu CR. Effects of sample geometry on the dynamics and configurations of vortices in mesoscopic superconductors. *Phys. Rev. B.* 2007; 76(2): 024509.

Maxwell E. Isotope effect in the superconductivity of mercury. *Phys. Rev*. 1950; 78(4): 477.

Meissner W and Ochsenfeld R. A new effect upon the onset of superconductivity. *Nat. Sci*. 1933; 21: 787-788.

Mel'nikov AS, Nefedov IM, Ryzhov DA, Shereshevskii IA, Vinokur VM and Vysheslavtsev PP. Vortex states and magnetization curve of square mesoscopic superconductors. *Phys. Rev. B*. 2002; 65(14): 140503.

Misko VR, Fomin VM, Devreese JT and Moshchalkov VV. Stable vortex-antivortex molecules in mesoscopic superconducting triangles. *Phys. Rev. Lett.* 2003; 90(14): 147003.

Misko VR, Xu B and Peeters FM. Formation and size dependence of vortex shells in mesoscopic superconducting niobium disks. *Phys. Rev. B.* 2007; 76(2): 024516.

Schweigert VA, Peeters FM and Deo PS. Vortex phase diagram for mesoscopic superconducting disks. *Phys. Rev. Lett.* 1998; 81(13): 2783.

Taupin M, Khaymovich IM, Meschke M, Mel'nikov AS and Pekola JP. Tunable quasiparticle trapping in Meissner and vortex states of mesoscopic superconductors. *Nat. Commun*. 2016; 7(1): 10977.

Tinkham M. Introduction to superconductivity. *Courier Corporation*, 2004. p 454.

Wang JS and Wang SY. High-Temperature superconductive maglev vehicle. *Endless Quests*: *Theory, experiments and applications of frontiers of superconductivity*. 2019; pp 249-314.

Zhao HJ, Misko VR, Peeters FM, Dubonos S, Oboznov V and Grigorieva IV. Vortex configurations in mesoscopic superconducting triangles: Finite-size and shape effects. *Europhys. Lett.* 2008; 83(1): 17008.

Zharkov GF, Zharkov VG and Zvetkov AY. Self-consistent solutions of Ginzburg-Landau equations and superconducting edge-suppressed states in magnetic field. *Phys. Rev. B.* 2000; 61(18):12293.